V European Conference on Computational Fluid Dynamics
ECCOMAS CFD 2010
J. C. F. Pereira and A. Sequeira (Eds)
Lisbon, Portugal,14-17 June 2010

DEVELOPMENT OF AN IMMERSED BOUNDARY METHOD USING BOUNDARY ELEMENTS WITHIN A VORTEX-IN-CELL/PARALLEL FAST MULTIPOLE METHOD

T. Lonfils*, G. Winckelmans

Université catholique de Louvain
Institute of Mechanics, Materials and Civil engineering (iMMC)
1348 Louvain-la-Neuve, Belgium
e-mail: timothee.lonfils@uclouvain.be
*F.R.I.A. Fellow

Key words: Vortex Method, Vortex-in-cell Method, Immersed boundary, External flows

Abstract. *This paper presents a method for the simulation of incompressible flows past arbitrary shape bodies. The method couples a combined vortex-in-cell (VIC) and parallel fast multipole (PFM) method to an Immersed Boundary (IB) approach. The Navier-Stokes equations in the vorticity-velocity formulation are solved. The Poisson equation for the streamfunction is solved efficiently in an unbounded domain by means of a direct solver; in each subdomain, the boundary conditions of which are provided by the PFM method which has a global view of the whole vorticity field.*

Because the vorticity field is a compact field, a very tight grid can be used and this makes an efficient method for unbounded vortical flows.

An IB method is used in order to easily deal with complex body geometries. In vorticity-velocity formulation, imposing the no-slip condition requires to solve a vector integral equation. This is done here using a boundary element method. The obtained panel strengths provide the equivalent vorticity flux at the wall.

The method has been successfully validated using a well-referenced test case, which consists in the flow past a sphere at $Re = 300$.

1 INTRODUCTION

We solve the Navier-Stokes equations for an incompressible flow in vorticity-velocity formulation. Those equations read

$$\frac{D\boldsymbol{\omega}}{Dt} = (\nabla \mathbf{u}) \cdot \boldsymbol{\omega} + \nu \nabla^2 \boldsymbol{\omega}, \tag{1}$$

where $\mathbf{u}$ is the velocity field and $\boldsymbol{\omega} \triangleq \nabla \times \mathbf{u}$ is the vorticity field. $\frac{D}{Dt} \triangleq \frac{\partial}{\partial t} + \mathbf{u} \cdot \nabla$ is, by definition, the material derivative. Using the Helmholtz decomposition, one can write the velocity field as

$$\mathbf{u} = \nabla \times \boldsymbol{\Psi} + \nabla \phi. \tag{2}$$

where $\boldsymbol{\Psi}$ is the so-called streamfunction and ϕ is the scalar potential. We take ϕ such that $\nabla \phi = \mathbf{U_0}$, where $\mathbf{U_0}$ is the upstream velocity. If we set the gauge of $\boldsymbol{\Psi}$ as $\nabla \cdot \boldsymbol{\Psi} = 0$, the vorticity field and the stream function are related by the Poisson equation

$$\nabla^2 \boldsymbol{\Psi} = -\boldsymbol{\omega}. \tag{3}$$

The vorticity field is discretized using vortex particles, responsible for a volume V_p and carrying a vorticity vector quantity ($\boldsymbol{\alpha}_p \triangleq \boldsymbol{\alpha}(\mathbf{x}_p) = \int_{V_p} \boldsymbol{\omega} dV \simeq \boldsymbol{\omega}(\mathbf{x}_p) V_p$). The evolution equations for the positions and the strengths of those particles read

$$\frac{d\boldsymbol{\omega}_p}{dt} = (\nabla \mathbf{u}(\mathbf{x}_p)) \cdot \boldsymbol{\omega}(\mathbf{x}_p) + \nu \nabla^2 \boldsymbol{\omega}(\mathbf{x}_p) \tag{4}$$

$$\frac{d\mathbf{x}_p}{dt} = \mathbf{u}(\mathbf{x}_p) \qquad \forall p = [1 \dots N] \tag{5}$$

Vortex particles methods require to solve Eq. (2) and (3) to obtain the velocity field from the particle strengths. For unbounded domains, Eq. (2) and (3) can be solved through fast summation techniques such as the Parallel Fast Multipole (PFM) method to reduce cost complexity from $\mathcal{O}(N^2)$ to $\mathcal{O}(N \log N)$. However these methods are still expensive for the simulation of external flows at practical Reynolds number (i.e. $\mathcal{O} > 10^3 \dots 10^4$). The presents approach takles this problem through the efficient combination of the "Vortex-In-Cell" (VIC, see[1]) method and the PFM method.

The advantage of VIC method is to solve the Poisson equation (Eq. (3)) using fast grid solvers that are much faster that Green's function based Poisson equation solver. The required boundary conditions are here provided by the PFM method instead of simplified analytical solution. Those boundary conditions being "exact", a very compact grid can be used, that is tight to the vorticity field. This is the basis of the hybrid VIC-PFM method. For parallel computing perspective, we note that no global Poisson equation is solved. Rather, multiple Poisson equations are solved locally on the Cartesian subgrid using the proper boundary conditions.

This hybrid scheme requires the source term of Eq. (3) to be available on the grid. This entails the translation of particles strength into a grid vorticity through interpolation. The

Right Hand Side (RHS) of Eq. (4) is computed using finite differences, thus efficiently. That requires, on the one hand, to interpolate particle strengths onto the grid in order to compute time-variation of each particle intensity and position. On the other hand, this "grid information" has to be interpolated from the grid to the particles. This method has been successfully developed by Cocle[2;3] for (half-)unbounded vortical flows.

This paper describes the extension of the VIC-PFM method in order to compute external flows past arbitrarily geometries at moderate Reynolds number. The methodology is based on an Immersed Boundary (IB) approach (first developed by R. Peskin[4], see also the review of Mittal *et al.*[5]).

Morgenthal *et al.*[6] have developed a 2-D immersed interface method for VIC algorithms. A influence matrix (Particle-Particle Particle-mesh algorithm, the PP^3M) is used in order to capture the under-resolved field. Cottet and Poncet[7], and Poncet[8] developed an IB method in a VIC code using potential sources instead of vorticity sources. The body surface is discretized over few grid points while, here, the surface is discretized using vortex panels in the spirits of sharp interface methods[9;10;11;12].

2 AN IMMERSED BOUNDARY METHOD WITHIN A VIC METHOD

The coupling of an IB method is well-suited for codes using velocity-pressure formulation because velocity components tend to zero at the wall. An IB method in a vorticity-based Navier-Stokes solver however has to handle a non-discontinuous field. Indeed, the vorticity is non zero on the fluid side an maximum at the wall and it is zero inside the body up to the wall. In the present approach the wall treatment relies on a symetrized vorticity field with respect to the wall.

The algorithm reads:

At time t^n, the vorticity field is discretized using a set $\mathcal{P}_1$ of particles characterized by their position and their strength: $(\mathbf{x}_p^n, \boldsymbol{\alpha}_p^n)$ for $p \in [1 \cdots N]$ where N is the number of particles. Moreover, the arbitrary body shape is discretized using a set $\mathcal{S}$ of panels forming a closed surface and described by the position of the three vertices: $(\mathbf{x}_{1,j}^n, \mathbf{x}_{2,j}^n, \mathbf{x}_{3,j}^n)$ for $j \in [1 \cdots M]$ where M is the number of panels.

1. **Random grid shifting.** The particle/panel position are randomly shifted between $-0.5h$ and $0.5h$, in each direction, in order to distribute the IB discretization error over the body surface. Indeed, the body discretization crosses arbitrarily the Cartesian grid. Hence, a non-uniform "discretization error" along the body is done.

2. **Mesh overlay.** A Cartesian grid with a uniform resolution h, is laid over the support of vorticity, i.e. it covers the location of all particles and panels.

3. **Wall distance.** The grid points are tagged relative to the wall distance. For each grid point $\mathbf{x}_{ijk} = (x_i, y_j, z_k) = (x_0 + ih, y0 + jh, z_0 + kh)$, a point $\mathbf{x}_{wall}$ on the wall surface exists such that $d = \min_{ijk}(|\mathbf{x}_{ijk} - \mathbf{x}_{wall}|)$, d is then the distance to the wall.

4. **Evaluation of the vorticity field on the grid.** We construct a set $\mathcal{P}_2$ of image vortex particles inside the body such that the spurious vorticity flux at the wall is minimized up to the curvature. The methodology is sketched in Fig. 1. The near-wall particle weight (i.e. $d/h < 0.5$ where d is the distance to the wall) has to be extrapolated from the flow. The weight is here computed using second-degree polynomial functions $\mathbf{P}$:

$$\left\{\begin{array}{rcl} \mathbf{P}_{t,n}(\mathbf{x}_{wall}+h\mathbf{n}) &=& \boldsymbol{\alpha}_{t,n}(\mathbf{x}_{wall}+h\mathbf{n}) \\ \mathbf{P}_{t,n}(\mathbf{x}_{wall}+2h\mathbf{n}) &=& \boldsymbol{\alpha}_{t,n}(\mathbf{x}_{wall}+2h\mathbf{n}) \\ \frac{\mathrm{d}\mathbf{P}_t}{\mathrm{dn}}(\mathbf{x}_{wall}) &=& 0 \text{ for tangential components} \\ \mathrm{P}_n(\mathbf{x}_{wall}) &=& 0 \text{ for normal component} \end{array}\right. \tag{6}$$

where $\mathrm{P}_n = \nabla\mathbf{P}\cdot\mathbf{n}$ and $\mathbf{P}_t = \mathbf{P} - \mathrm{P}_n\mathbf{n}$.

Afterward, the weight of the particle sets ($\mathcal{P}_1$ and $\mathcal{P}_2$) are redistributed onto the grid using the $M_4^{'}$ scheme:

$$\boldsymbol{\alpha}_p^n \xrightarrow{M_4^{'}} \boldsymbol{\alpha}_{ijk}^n. \tag{7}$$

More precisely,

$$\boldsymbol{\alpha}_{ijk}^n = \sum_{p=0}^{N} M_4^{'}(x_i - x_p)\, M_4^{'}(y_j - y_p)\, M_4^{'}(z_k - z_p)\, \boldsymbol{\alpha}_p^n. \tag{8}$$

where,

$$M_4^{'}(x) = \left\{\begin{array}{ll} 1 - \frac{5}{2}|x|^2 + +\frac{3}{2}|x|^3, & |x| \le 1, \\ \frac{1}{2}(2-|x|)^2(1-|x|), & 1 < |x| < 2, \\ 0, & |x| \ge 0. \end{array}\right. \tag{9}$$

The $M_4^{'}$ scheme has very good conservation properties, see Monaghan[13], Cotted and Koumoutsakos[14] and Winckelmans[15]. Moments up to the second (i.e. the vorticity, the linear impulse and the angular impulse) are conserved.

The redistribution is also used to handle Lagrangian distorsion in particle methods. With time, particles tend to cluster or deplete some region of the flow (e.g. recirculation zone), thus causing a loss of overlap between particles. Redistribution proceeds by periodically generating a new set of particles (from the old set) on a regular lattice.

5. **No-slip condition.** The vortex panel vector intensity is computed such that the tangential vector velocity underneath each panel is canceled (see Fig. 2).

Imposing the no-slip flow condition at the wall requires to solve a vector integral equation. This is done here using a Boundary Element Method (BEM). For vortex

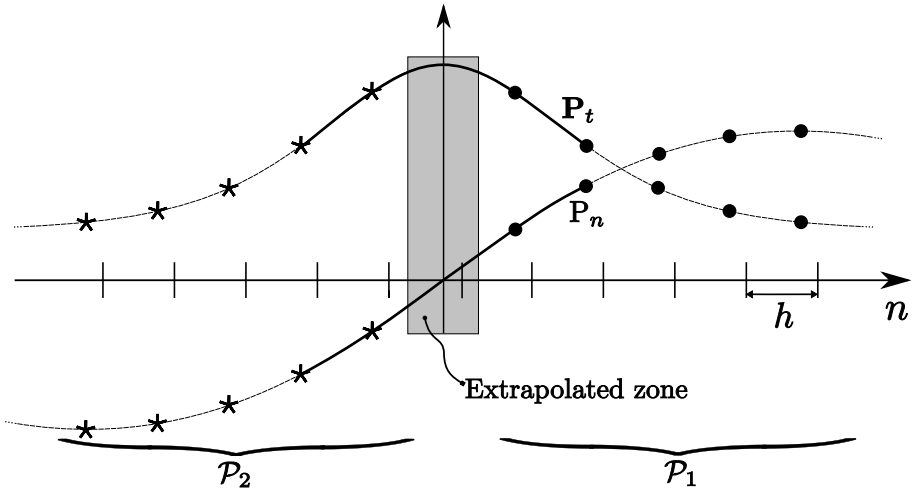

Figure 1: General description of the methodology computing the near-wall vorticity field in the local reference frame. The "bullets" ($\bullet$) and the "stars" ($*$) respectively represent the set $\mathcal{P}_1$ of outer-body particles and the set $\mathcal{P}_2$ of inner-body particles.

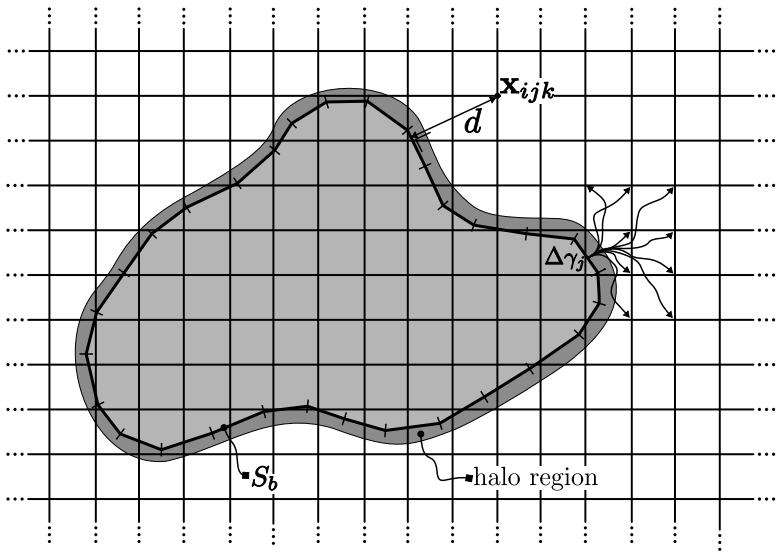

Figure 2: General description of the IB method.

panels of vector strength $\Delta\boldsymbol{\gamma}$:

$$\begin{aligned}\frac{1}{2}\Delta\boldsymbol{\gamma}(\mathbf{x})\times\mathbf{n}+\frac{1}{4\pi}\int_S \frac{1}{|\mathbf{x}-\mathbf{x}'|^3}\cdot(\mathbf{x}-\mathbf{x}')\times\Delta\boldsymbol{\gamma}\; dS(\mathbf{x}') &= \mathbf{U}_0+\mathbf{u}_\omega(\mathbf{x}) \\ &= \Delta\mathbf{U}_{slip} \qquad (10)\end{aligned}$$

where $\mathbf{u}_\omega$ is the solution of Eq. (2) and (3), the vortex-field induced velocity. This equation is solved using an iterative method (a under-relaxed modified-Jacobi algorithm). The surface body is discretized using triangles. In order to reduce memory and computational cost, the matrix-vector multiplications (i.e. particle-panel and panel-panel interactions) in the linear solver are evaluated by means of the PFM method. The PFM method is, in practice, required in order to evaluate the particle-panel interactions and the panel-panel interactions.

The RHS, i.e. the residual velocity $\Delta\mathbf{U}_{slip}$, is also evaluated using the PFM method. The particles are considered for this step as "point" particles so as to have an entire view of the vorticity field. A "halo" region, where no particle can exist, is defined to avoid spurious vorticity flux at the wall. Typically, one fixes $d_{halo}/h = 0.20\cdots0.25$. Particles entering in this zone are reflected.

6. **Vortcity flux.** A Lighthill's model of vorticity flux at the wall is used[14;16;17]. For each grid point $\mathbf{x}_{ijk}$, the net circulation increase $\Delta\boldsymbol{\alpha}^n_{ijk,cons}$, due to the diffusion of the vortex panels within the flow, is computed using a conservative scheme. Let's consider a panel with an area Ω and intensity $\Delta\boldsymbol{\gamma}$. One defines an infinitesimal surface $dS = d\xi\, d\eta$, the net circulation increase over a time Δt is given by the following formula

$$\Delta\boldsymbol{\alpha}_{ijk} = \int_0^1 \frac{\mathrm{d}\boldsymbol{\alpha}_{ijk}}{\mathrm{d}(t/\Delta t)}\mathrm{d}(t/\Delta t),$$

where

$$\begin{aligned}\frac{\mathrm{d}\boldsymbol{\alpha}_{ijk}}{\mathrm{d}(t/\Delta t)} &= \frac{1}{2}\Delta\boldsymbol{\gamma}\left([\mathrm{erfc}(u)]^{(z_k-h_l/2)/\sqrt{4\nu t}}_{(z_k+h/2)/\sqrt{4\nu t}}\right) \\ &\quad \int_S [\mathrm{erfc(u)}]^{(x_i-h/2-x(\xi,\eta))/\sqrt{4\nu t}}_{(x_i+h/2-x(\xi,\eta))/\sqrt{4\nu t}} [\mathrm{erfc(u)}]^{(y_j-h/2-y(\xi,\eta))/\sqrt{4\nu t}}_{(y_j+h/2-y(\xi,\eta))/\sqrt{4\nu t}} \underbrace{d\xi\, d\eta}_{dS}. \qquad (11)\end{aligned}$$

ξ and η are the local integration coordinates. h_l is equal to zero if $z_k < h/2+d_{halo}$ and is $h/2$ else. This formula is numericaly integrated i) in-time using four-point Gauss quadrature and ii) over the triangle using the three-point hammer rule. Notice that this formula can be analyticaly integrated if the panel is a rectangle ($S = f \times b$).

Eq. (11) can be rewriten as followed

$$\begin{aligned}\frac{\mathrm{d}\boldsymbol{\alpha}_{ijk}}{\mathrm{d}(t/\Delta t)} &= \nu t \Delta\boldsymbol{\gamma} \left([\mathrm{erfc}(u)]_{(z_k+h/2)/\sqrt{4\nu t}}^{(z_k-h_l/2)/\sqrt{4\nu t}} \right) \\ &\left([\mathrm{ierfc(u)}]_{(x_i-h/2-b/2)/\sqrt{4\nu t}}^{(x_i+h/2-b/2)/\sqrt{4\nu t}} - [\mathrm{ierfc(u)}]_{(x_i-h/2+b/2)/\sqrt{4\nu t}}^{(x_i+h/2+b/2)/\sqrt{4\nu t}} \right) \\ &\left([\mathrm{ierfc(u)}]_{(y_j-h/2-f/2)/\sqrt{4\nu t}}^{(y_j+h/2-f/2)/\sqrt{4\nu t}} - [\mathrm{ierfc(u)}]_{(y_j-h/2+f/2)/\sqrt{4\nu t}}^{(y_j+h/2+f/2)/\sqrt{4\nu t}} \right). \end{aligned} \quad (12)$$

In practice, if the triangular panels are equilateral enough, the panels considered as rectangular (i.e. $f \triangleq b \triangleq \sqrt{S_\triangle}$). Moreover, the scheme can be made conservative through a weighted correction developed by Ploumhans *et al.*[17], is used

$$\Delta\boldsymbol{\alpha}_{ijk,cons} = \Delta\boldsymbol{\alpha}_{ijk} + \frac{|\Delta\boldsymbol{\alpha}_{ijk}|^2}{\sum_{r,s,t} |\Delta\boldsymbol{\alpha}_{(r,s,t)}|^2} \left(S\Delta\boldsymbol{\gamma} - \sum_{r,s,t} \Delta\boldsymbol{\alpha}_{(r,s,t)} \right).$$

7. **Poisson equation.** Solving the Poisson equation $\nabla^2 \boldsymbol{\Psi}_{ijk}^n = -(\boldsymbol{\omega}_{ijk}^n + \Delta\boldsymbol{\omega}_{ijk}^n)/(h^3)$ using the mathematical library `FISHPACK` (for more details, see[18;19;20]). Required boundary conditions are obtained using the PFM method. The vortex panel intensity is first redistributed onto the grid before solving the Poisson equation $\nabla^2\boldsymbol{\Psi} = -\boldsymbol{\omega}$, then diffused to the near-wall particles (see[17]).

8. **Evolution equation.** Computing is done using Finite Differences (FD)

$$\mathbf{u}_{ijk}^n = \nabla \times \boldsymbol{\Psi}_{ijk}^n$$

and

$$\frac{d\boldsymbol{\omega}_{ijk}^n}{dt} = (\nabla \mathbf{u}_{ijk}^n).\boldsymbol{\omega}_{ijk}^n + \nu\nabla^2\boldsymbol{\omega}_{ijk}^n.$$

Notice that the velocity and the stretching term is computed using centered second-order FD. The diffusion term is computed using a 27 points "cube" scheme instead of the "cross" scheme (see[3]), it provides less sensitivity to the grid.

9. **Vorticity divergence.** With time, the vorticity field does not remain an "image" of the velocity curl for several reasons. i) The interpolation procedure (particle-mesh, mesh-particle) using the $M_4^{'}$ scheme, does not conserve the divergence of the vorticity field. ii) The stream function $\boldsymbol{\Psi}$ obtained by solving the Poisson equation, using `FISHPACK`, is not divergence free. Moreover, a "collocated" lattice instead of a "staggered" lattice is used. The numerical scheme is thus not fully consistent: the numerical Laplacian operator does not match with the numerical double rotational operator ($\nabla_h \times (\nabla_h \times \boldsymbol{\Psi}) \neq -\nabla_h^2 \boldsymbol{\Psi} = \boldsymbol{\omega}$).
The vorticity field thus has to be regularly corrected in order to project it in a divergence free space, following a methodology first developed by Cotted and Poncet[7], and Poncet[21].

The vorticity field $\boldsymbol{\omega}$ can be corrected to a divergence free field $\tilde{\boldsymbol{\omega}}$:

$$\tilde{\boldsymbol{\omega}} = \boldsymbol{\omega} - \nabla D, \tag{13}$$

by simply taking D such that

$$\nabla^2 D = \nabla \cdot \boldsymbol{\omega}. \tag{14}$$

Moreover, the existence of a wall requires to solve a scalar integral equation, over the wall surface, to impose the following boundary condition

$$\tilde{\boldsymbol{\omega}} \cdot \mathbf{n} = 0 \Leftrightarrow \nabla D \cdot \mathbf{n} = \boldsymbol{\omega} \cdot \mathbf{n}. \tag{15}$$

Notice that the Poisson equation is solved using the same combination of the `FISHPACK` library and the PFM method. For the same reason that the vorticity field is not exactly divergence free (consistency between Laplacian operator versus double rotational operator), the above correction scheme (Eq. (14) and (13)) does not exactly provide a solenoidal field. However, it turns out that this step provides satisfactory results, if the vorticity field is smooth enough.

Moreover the near-wall vorticity field is often locally under-resolved, due to the "halo" region, the evaluation of the divergence sources leads to spurious corrections of the vorticity field. For this reason, the near-wall divergence sources (i.e. $d < 2h$) and the boundary condition are not taken into account during this correction step.

10. **Interpolation.** Grid quantities (i.e. velocity, time-derivative of strength and net increase of intensity due to panel diffusion) are interpolated onto the particles using the M_4' scheme

$$\begin{aligned}
\mathbf{u}_{ijk}^n &\xrightarrow{M_4'} \mathbf{u}_p^n \\
\left(\frac{d\boldsymbol{\alpha}}{dt}\right)_{ijk}^n &\xrightarrow{M_4'} \left(\frac{d\boldsymbol{\alpha}}{dt}\right)_p^n \\
\Delta\boldsymbol{\alpha}_{ijk}^n &\xrightarrow{M_4'} \Delta\boldsymbol{\alpha}_p^n
\end{aligned}$$

11. **Time integration.** The particle positions and strengths are integrated in time using respectively the Leap-Frog scheme and the second-order Adams-Bashford (AB) scheme

$$\begin{aligned}
\mathbf{x}_p^{n+1} &= \mathbf{x}_p^{n-1} + 2\Delta t \mathbf{u}_p^n. \\
\boldsymbol{\alpha}_p^{n+1} &= \boldsymbol{\alpha}_p^n + \frac{1}{2}\Delta t \left(3\left(\frac{d\boldsymbol{\alpha}}{dt}\right)_p^{n-1} - \left(\frac{d\boldsymbol{\alpha}}{dt}\right)_p^n\right) + \Delta\boldsymbol{\alpha}_p^n \\
t^{n+1} &= t^n + \Delta t.
\end{aligned}$$

After particle redistribution, the AB temporal integration scheme cannot be used anymore and is replaced by the second order Runge-Kutta scheme
The first step (predictor) is

$$\begin{aligned} \mathbf{x}_p^* &= \mathbf{x}_p^n + \Delta t \mathbf{u}_p^n \\ \boldsymbol{\alpha}_p^* &= \boldsymbol{\alpha}_p^n + \Delta t \left(\frac{d\boldsymbol{\alpha}}{dt}\right)_p^n + \Delta \boldsymbol{\alpha}_p^n \\ t^* &= t^n + \Delta t, \end{aligned}$$

and the second step (corrector) is

$$\begin{aligned} \mathbf{x}_p^{n+1} &= \mathbf{x}_p^n + \frac{1}{2}\Delta t \left(\mathbf{u}_p^n + \mathbf{u}_p^*\right) \\ \boldsymbol{\alpha}_p^{n+1} &= \boldsymbol{\alpha}_p^n + \frac{1}{2}\Delta t \left(\left(\frac{d\boldsymbol{\alpha}}{dt}\right)_p^n + \left(\frac{d\boldsymbol{\alpha}}{dt}\right)_p^* + \frac{\Delta \boldsymbol{\alpha}_p^*}{\Delta t}\right) \\ t^{n+1} &= t^*. \end{aligned}$$

3 VALIDATION

The present VIC-PFM-IB methodology has been validated on a well-known test case for which experimental and numerical data are available: the flow past a sphere at $Re = \frac{U_0 D}{\nu} = 300$. At such a Reynolds number, the flow is known to be unsteady, thus making it a relevant test for our handling of the no-slip condition and the diffusion step.

The mesh resolution is here fixed to $h/D = 1.0/75$ and the time step is $\Delta t U_0/D \leq 1.25\,10^{-2}$. The wake is simulated up to 20 diameters downstream. The sphere is discretized using 20 480 quasi-equilateral triangles obtained by recursive subdivision of an icosahedron. The average surface of the triangles is $\sqrt{\overline{S_\triangle}}/h = 0.93$. Fig. 4 shows various views of the wake behind the sphere. The vortical structure, the so-called "hairpin" vortices, are clearly present (here visualized using the λ_2 criterion[22]. Fig. 5 shows a 2-D cut of the vorticity field for the entire flow (a) and a zoom in the near-wall region (b).

The force acting on a body can be computed from an exact formula developed by Noca *et al.*[23;24] and applied to PIV (Particle Image Velocitmetry) measurements. This formula was also successfully used in the context of vortex particle method by Ploumhans *et al.*[17] and Daeninck[25]. Let us consider a control volume V_C with a surface S_C which includes the body described by the simply-connected closed surface S_b, see Fig. 3. The force acting

on S reads

$$\begin{aligned}\frac{\mathbf{F}}{\rho} &= -\frac{1}{\mathcal{N}-1}\frac{d}{dt}\int_{S_C+S_b}\left((\mathbf{u}\cdot\mathbf{x})\mathbf{n}-\mathbf{u}(\mathbf{x}\cdot\mathbf{n})+(\mathcal{N}-1)\mathbf{x}(\mathbf{u}\cdot\mathbf{n})\right)dS \\ &+\int_{S_C}\left(\frac{1}{2}(\mathbf{u}\cdot\mathbf{u})\mathbf{n}-(\mathbf{n}\cdot\mathbf{u})\mathbf{u}\right)dS \\ &-\frac{1}{\mathcal{N}-1}\int_{S_C}(\mathbf{n}\cdot\mathbf{u})(\mathbf{x}\times\boldsymbol{\omega})dS+\frac{1}{\mathcal{N}-1}\int_{S_C}(\mathbf{n}\cdot\boldsymbol{\omega})(\mathbf{x}\times\mathbf{u})dS \\ &+\frac{1}{\mathcal{N}-1}\int_{S_C}\mathbf{x}\times(\mathbf{n}\times\nabla\cdot\mathbf{T})dS+\int_{S_C}\mathbf{n}\cdot\mathbf{T}dS, \end{aligned} \tag{16}$$

where $\mathbf{T}=\nu\left(\nabla\mathbf{u}+(\nabla\mathbf{u})^T\right)$. This formula is particularly well adapted for vortex method, because it only requires the knowledge of the velocity and its derivatives; the pressure field is not required. Note that the surface integral on S_b vanishes when $\mathbf{u}=\mathbf{0}$ at the wall (as for the flows considered in this paper). The evaluation of the various fields are thus only needed on the control surface S_C.

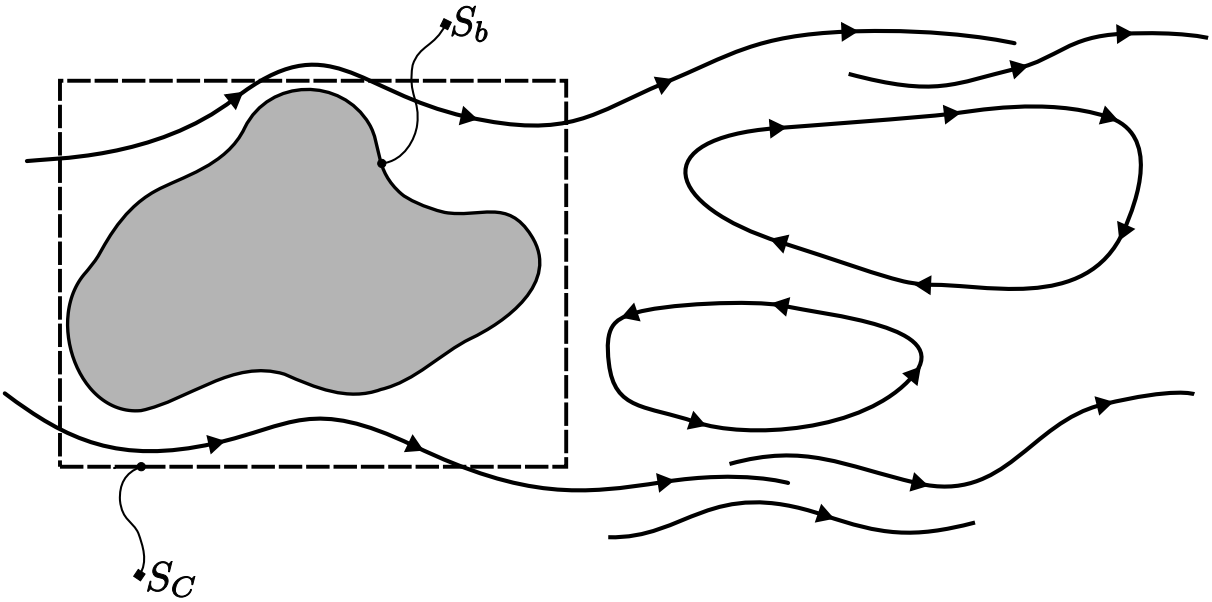

Figure 3: General view of the flow past an arbitrarily shape.

One defines the Drag coefficient (C_D)

$$C_D=\frac{\mathbf{F}\cdot\mathbf{e_y}}{\frac{1}{2}\rho U_0^2(\pi D^2/4)} \tag{17}$$

	$\overline{C_D}$	ΔC_D	$\overline{C_L}$	ΔC_L	Str
Present work	0.672	$3.4\,10^{-3}$	0.065	$1.5\,10^{-2}$	0.134
Johnson & Patel[26]	0.656	$3.5\,10^{-3}$	0.069	$1.6\,10^{-2}$	0.137
Tomboulides & Orszag[27]	0.671	$2.8\,10^{-3}$	-	-	0.137
Constantinescu *et al.*[28]	0.655	-	0.065	-	0.136
Ploumhans *et al.*[17]	0.683	$2.5\,10^{-3}$	0.061	$1.4\,10^{-2}$	0.135
Georges[29]	0.661	$2.5\,10^{-3}$	0.066	$1.3\,10^{-2}$	0.134

Table 1: Summarizing table of interest quantities compared to the literature for the flow past a sphere at Reynolds 300.

where $\mathbf{e_y}$ is the streamwise unit vector. The Lift coefficient (C_L) is defined as

$$C_L = \frac{||\mathbf{F} - (\mathbf{F}\cdot\mathbf{e_y})\mathbf{e_y}||}{\frac{1}{2}\rho U_0^2(\pi D^2/4)} \tag{18}$$

The time-evolution of the diagnostics (drag/lift coefficients) are presented in Fig. 6. Table 1 shows a brief comparison with reference results. The time-averaged value of C_D and C_L, as well as the Strouhal number($Str = f\,D/U_0$), compare well with those of the literature. As for the oscillation amplitude ($\Delta C_D \triangleq \frac{1}{2}(\max C_D - \min C_D)$ and $\Delta C_L \triangleq \frac{1}{2}(\max C_L - \min C_L)$), they compare quite well with those of the literature. It is worth noting that those latter values are more difficult to obtain.

Along the simulation, the mesh Reynolds number, based on the vorticity field ($Re^{\boldsymbol{\omega}}_{mesh} = \frac{\max(|\boldsymbol{\omega}|)h^2}{\nu}$) or based on the velocity field ($Re^{\mathbf{u}}_{mesh} = \frac{\max(|\mathbf{u}|)h}{\nu}$), was maintained at a low level $\mathcal{O}(5\cdots 7)$, see Fig. 7.(a). Moreover, the divergence of the vorticity field was also maintained at an acceptable level $\mathcal{O}(5\,10^{-4})$, see Fig. 7.(b).

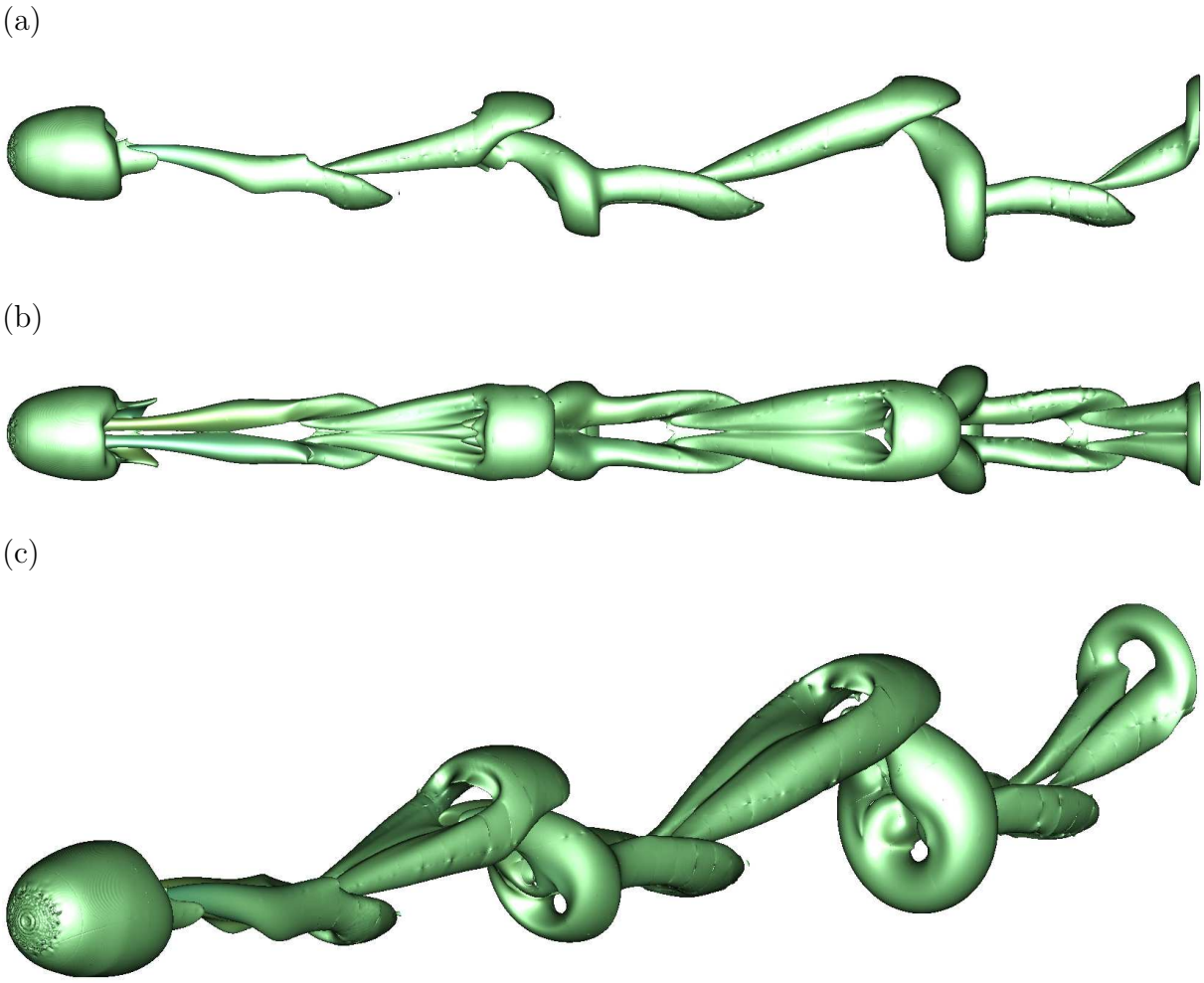

Figure 4: Isocontour of the λ_2 criterion: (a) top view, (b) side view and (c) offset view.

(a)

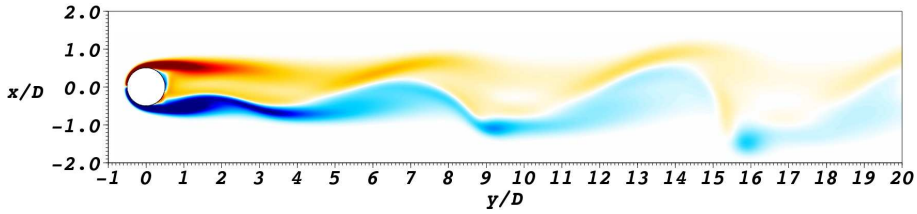

(b)

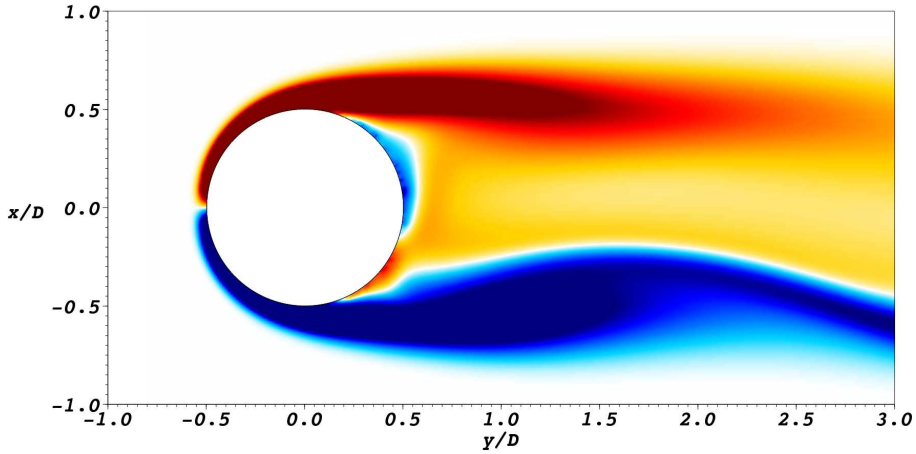

Figure 5: 2D slice of the z-component of the vorticity field $\frac{D}{U_0}\boldsymbol{\omega}$: (a) global view and (b) zoom in the near-wall region. Saturation was used in order to see both the near wall vorticity and the wake vorticity.

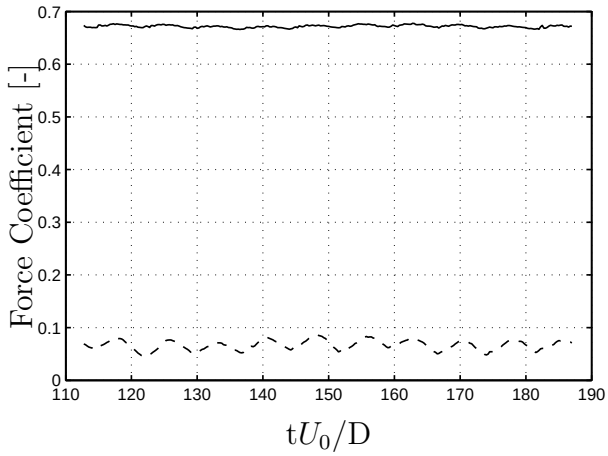

Figure 6: Time-evolution of the force acting on the sphere: drag coefficient (solid line) and lift coefficient (dashed line).

(a) (b)

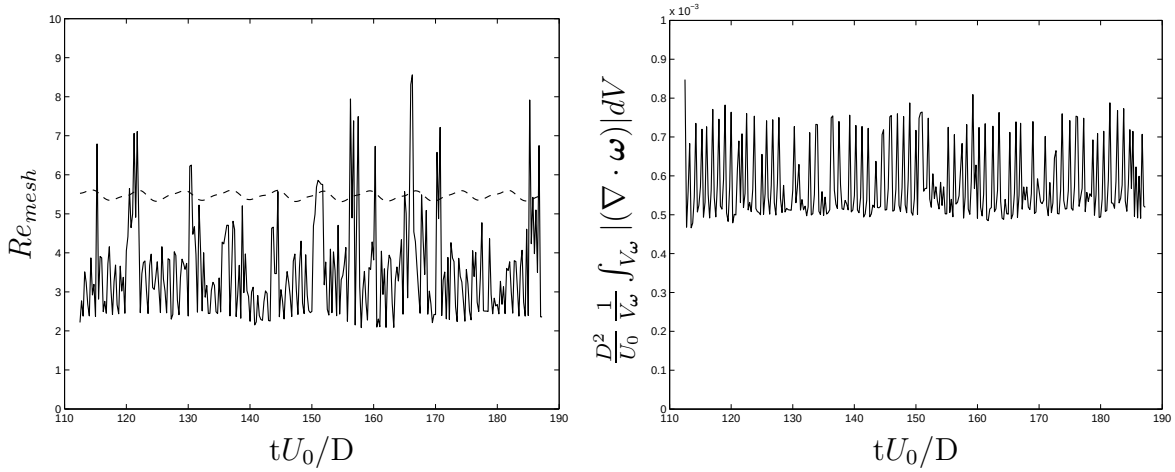

Figure 7: (a) Time-evolution of the mesh Reynolds number $Re^{\boldsymbol{\omega}}_{mesh}$ (solid line) and $Re^{\mathbf{u}}_{mesh}$ (dashed line). (b) Time-evolution of the divergence of the vorticity field. $V_{\boldsymbol{\omega}}$ is the volume where $\boldsymbol{\omega}$ is non zero.

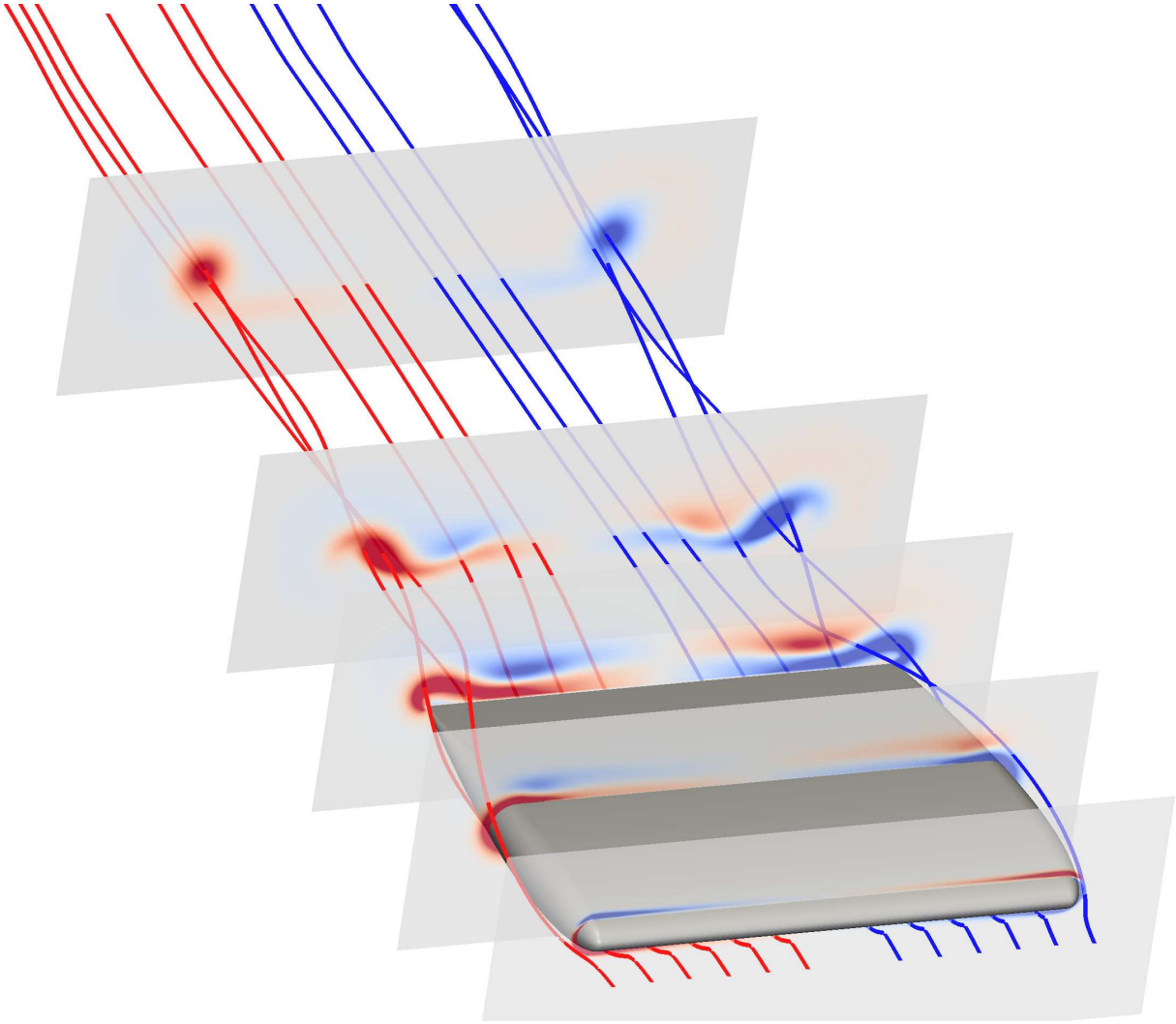

Figure 8: Streamlines and streamwise vorticity cut-planes of the flow past a low aspect-ratio wing (NACA0012 profile).

4 CONCLUDING REMARKS

The presented IB method within the VIC-PFM method provides satifstactory results for the simulation of the flows past arbitrary body shape, at moderate Reynolds number, in terms of flow dynamics and forces acting on the body.

The IB approach conserves the main advantages of the VIC-PFM method[3], that is, i) the easy and efficient paralellization of any problem by locally solving the Poisson equation on each subdomain.

The method has been successfully validaded against the test case of the flow past a sphere at $Re = 300$. Satisfactory results were obtained.

Recently, the method has also been successfully applied to the simulation of the impulsively started flow past a very low aspect-ratio wing (NACA0012 profile, $AR = 1$) at moderate Reynolds number ($Re = cU_0/\nu = 3000$ where c is the chord). The wing surface was discretized using 152 000 triangular panels. The complete formation of lift-induced vortices is captured (see Fig. 8). The method was seen to be robust; in particular, it can be weakly under-resolved locally.

So far, the method uses uniform isotropic grids. The extension to a multi-resolution framework is ongoing work.

5 ACKNOWLEDGMENTS

T. Lonfils is supported by the F.R.I.A. (Fond pour la Recherche en Industrie et Agriculture) fellowship funded by the Belgian french community F.R.S.-FNRS (Fond de la Recherche Scientifique). The authors are grateful to CENAERO (Center of Excellence in Aeronautical Research) which provides access to their high performance computing facility.

5 REFERENCES

[1] J. P. Christiansen. Numerical solution of hydrodynamics by the method of point vortices. *J. Comp. Phys.*, 13:363–379, 1973.

[2] R. Cocle. *Combining the vortex-in-cell and parallel fast multipole methods for efficient domain decomposition simulations : DNS and LES approaches*. PhD thesis, Université catholique de Louvain, Louvain-la-Neuve, 2007.

[3] R. Cocle, G. Winckelmans, and Daeninck. Combining the vortex-in-cell and parallel fast multipole methods for efficient domain decomposition simulations. *J. Comp. Phys.*, 227:2263–2292, 2008.

[4] C.S. Peskin. The immersed boundary method. *Acta Numerica*, pages 479–517, 2002.

[5] R. Mittal and G. Iaccarino. Immersed boundary methods. *Annu. Rev. Fluid Mech.*, 37:239–261, 2005.

[6] G. Morgenthal and J.H. Walther. An immersed interface method for the vortex-in-cell algorithm. *Comput. Struct.*, 85(11-14):712–726, 2007. ISSN 0045-7949. doi: http://dx.doi.org/10.1016/j.compstruc.2007.01.020.

[7] G.-H. Cottet and P. Poncet. Advances in direct numerical simulations of 3d wall-bounded flows by vortex-in-cell methods. *J. Comput. Phys.*, 193(1):136–158, 2004. ISSN 0021-9991. doi: http://dx.doi.org/10.1016/j.jcp.2003.08.025.

[8] P. Poncet. Analysis of an immersed boundary method for three-dimensional flows in vorticity formulation. *J. Comput. Phys.*, 228:7268–7288, 2009.

[9] H.S. Udaykumar, R. Mittal, P. Rampunggoon, and A. Khanna. A sharp interface cartesian grid method for simulating flows with complex moving boundaries. *Journal of Computational Physics*, 174(1):345 – 380, 2001. ISSN 0021-9991. doi: DOI: 10.1006/jcph.2001.6916.

[10] S. Marella, S. Krishnan, H. Liu, and H.S. Udaykumar. Sharp interface cartesian grid method i: An easily implemented technique for 3d moving boundary computations. *Journal of Computational Physics*, 210(1):1 – 31, 2005. ISSN 0021-9991. doi: DOI: 10.1016/j.jcp.2005.03.031.

[11] H. Liu, S. Krishnan, S. Marella, and H.S. Udaykumar. Sharp interface cartesian grid method ii: A technique for simulating droplet interactions with surfaces of arbitrary shape. *Journal of Computational Physics*, 210(1):32 – 54, 2005. ISSN 0021-9991. doi: DOI: 10.1016/j.jcp.2005.03.032.

[12] Y. Yang and H.S. Udaykumar. Sharp interface cartesian grid method iii: Solidification of pure materials and binary solutions. *Journal of Computational Physics*, 210 (1):55 – 74, 2005. ISSN 0021-9991. doi: DOI: 10.1016/j.jcp.2005.04.024.

[13] J.J Monaghan. Extrapolating b splines for interpolation. *Journal of Computational Physics*, 60(2):253 – 262, 1985. ISSN 0021-9991. doi: DOI: 10.1016/0021-9991(85)90006-3.

[14] G.H. Cottet and P.D. Koumoutsakos. *Vortex Methods: Theory and Practice.* Cambridge University Press, first edition, 2000.

[15] G.S. Winckelmans. Vortex methods. In E. Stein, R. de Borst, and T.J.R Hughes, editors, *Encyclopedia of computational mechanics*, volume 3 (Fluids). John Wiley & sons, 2004.

[16] P. Ploumhans and G. S. Winckelmans. Vortex methods for high-resolution simulations of viscous flow past bluff bodies of general geometry. *J. Comp. Phys.*, 165: 354–406, 2000.

[17] P. Ploumhans, G. S. Winckelmans, J. K. Salmon, A. Leonard, and M. S. Warren. Vortex methods for direct numerical simulation of three-dimensional bluff body flows: application to the sphere at Re = 300, 500, and 1000. *J. Comput. Phys.*, 178(2):427–463, 2002. ISSN 0021-9991. doi: http://dx.doi.org/10.1006/jcph.2002.7035.

[18] P.N. Swarztrauber and R.A. Sweet. The fourier and cyclic reduction methods for solving Poisson's equation. In J.A. Schetz and A.E. Fuhs, editors, *Handbook of fluid dynamics and fluid machinery.* John Wiley & Sons, New York, 1996.

[19] P.N. Swarztrauber. A direct method for the discrete solution of separable elliptic equations. *SIAM Journal of Numerical Analysis*, 11:1136–1150, 1974.

[20] P.N. Swarztrauber, R. A. Sweet, and J. C. Adams. FISHPACK: Efficient FORTRAN Subprograms for the Solution of Elliptic Partial Differential Equations. Technical report, National Center for Atmospheric Research, http://www.cisl.ucar.edu/css/software/fishpack/technote.ps, July 1999.

[21] P. Poncet. Vanishing of mode b in the wake behind a rotationally oscillating circular cylinder. *Physics of Fluids*, 14(6):2021–2023, 2002. doi: 10.1063/1.1479344.

[22] J. Jeong and F. Hussain. On the identification of a vortex. *Journal of Fluid Mechanics Digital Archive*, 285(-1):69–94, 1995.

[23] F. Noca, D. Shiels, and D. Jeon. Measuring instantaneous fluid dynamic forces on bodies, using only velocity fields and their derivatives. *Journal of Fluids and Structures*, 11(3):345 – 350, 1997. ISSN 0889-9746. doi: DOI: 10.1006/jfls.1997.0081.

[24] F. Noca, D. Shiels, and D. Jeon. A comparison of methods for evaluating time-dependent fluid dynamic forces on bodies, using only velocity fields and their derivatives. *Journal of Fluids and Structures*, 13(5):551 – 578, 1999. ISSN 0889-9746. doi: DOI: 10.1006/jfls.1999.0219.

[25] G. Daeninck. *Developments in hybrid approaches, Vortex method with known speration location, Vortex method with near-wall Eulerian solver, RANS-LES coupling.* PhD thesis, Université catholique de Louvain, Louvain-la-Neuve, 2006.

[26] T. A. Johnson and V. C. Patel. Flow past a sphere up to a Reynolds number of 300. *Journal of Fluid Mechanics*, 378(-1):19–70, 1999. doi: null.

[27] A. G. Tomboulides and S. A. Orszag. Numerical investigation of transitional and weak turbulent flow past a sphere. *Journal of Fluid Mechanics*, 416(-1):45–73, 2000.

[28] G. Constantinescu and K. Squires. Numerical investigations of flow over a sphere in the subcritical and supercritical regimes. *Physics of Fluids*, 16(5):1449–1466, 2004. doi: 10.1063/1.1688325.

[29] L. Georges. *Development and validation of a LES methodology for complex wall-bounded flows : application to high-order structured and industrial unstructured solvers.* PhD thesis, Université catholique de Louvain, Louvain-la-Neuve, 2007.